NJC

PAPER

View Article Online
View Journal | View Issue

Cite this: *New J. Chem.*, 2019, **43**, 19355

Self-assembly and photo-responsive behavior of bis-terpyridyl Eu^{3+}-complex L1†

Chuan Dong,[a] Jin Yuan,[a] Heinz Hoffmann[b] and Jingcheng Hao *[a]

Received 16th August 2019,
Accepted 12th November 2019

DOI: 10.1039/c9nj04252k

rsc.li/njc

In the present paper, a bis-terpyridyl Eu^{3+} complex (**bis-terpyridyl Eu^{3+}-complex L1**) was synthesized through the coordination between Eu^{3+} and a **compound L1** with an azobenzene-functionalized chain between the two terpyridine ligands. The assembly behavior of **bis-terpyridyl Eu^{3+}-complex L1**, which could be an excellent ultraviolet-responsive luminescent material, was investigated. We found that the introduction of an azobenzene-functionalized chain between bis-terpyridine ligands enabled the Eu^{3+} complex to undergo photo-isomerization and control the aggregation behavior in a solution. Upon irradiation by 365 nm ultraviolet light, the methanol solution of the Eu^{3+}complex exhibited visible fluorescence enhancement with an order of magnitude improvement in the fluorescence quantum yield and fluorescent lifetime. In particular, the photo-induced isomerization of azobenzene induced the transition of aggregates from nanospheres to micron sheets. The transition of aggregates was demonstrated by dynamic laser light scattering (DLS) data, atomic force microscopy (AFM) observations and Gaussian simulations. After UV irradiation, the tight accumulation of fluorophores in **bis-terpyridyl Eu^{3+}-complex L1** was speculated to be the dominant factor of the enhanced photoluminescence property. Our study may help expand the research on azobenzene-functionalized molecules based on coordination and provide a promising way for preparing responsive fluorescent materials.

1. Introduction

Fluorescent materials, especially organic fluorescent molecules, have attracted much attention due to their wide applications in bioimaging,[1–4] chemosensing,[5–7] and fluorescence analysis.[8,9] In principle, both monomer molecules and self-assembled aggregates can be used to construct fluorescent materials. Most of the conventional organic fluorophores with polycyclic aromatic hydrocarbon groups such as fluorescein and rhodamine suffer fluorescence inhibition or optical quenching at high concentrations.[10] This so-called aggregation-caused quenching (ACQ) effect reduces the quantum yield[11] and limits the applications of the molecules. As a breakthrough against this structural constraint, fluorescent materials with aggregation-induced emission (AIE) opposite to those with ACQ were first reported by Tang *et al.* in 2001,[12] and they have rapidly attracted growing interest due to the unique light-emitting mechanism. Compared to classic fluorophores, the rotor-like AIE molecules exhibit significant emission enhancement in the solid state or after aggregation. A restriction of intramolecular rotation decreases the non-radiative decays through molecular motions and enhances the emission intensity.[13,14] However, the fabrication of AIE molecules suffers from complicated molecular synthesis and the limitation of the rotor-like functional groups such as tetraphenyl ethylene (TPE).

Another significant strategy to fabricate luminescent materials involves combining metal ions with organic ligands *via* coordination.[15–17] Known as splendid tridentate ligands with fluorescence, terpyridyl derivatives have been utilized in preparing metal–organic luminescent materials for a long time.[18,19] Due to the three N centers formed *via* thermodynamic chelation, the construction of terpyridyl-metal coordination has good stability. The terpyridyl group exhibits excellent electron absorption capacity to transition and rare-earth metal ions by forming a relationship of a σ lectron donor and a π-receptor. At present, the research of responsive terpyridyl-metal-coordinated luminescent materials mainly concentrates on the replacement of metal ions, but the terpyridyl derivatives with responsive chemical groups are rarely reported.

In this paper, a coordinative **compound L1** with an azobenzene-functionalized chain between two terpyridine ligands was synthesized. We investigated the detailed aggregation process of **bis-terpyridyl Eu^{3+}-complex L1** formed between **compound L1** molecules and Eu^{3+} ions in the mixed solvent of dichloromethane and methanol (v:v = 1:1). The photo-responsive aggregation fluorescence of **bis-terpyridyl Eu^{3+}-complex L1**

[a] *Key Laboratory of Colloid and Interface Chemistry & Key Laboratory of Special Aggregated Materials, Shandong University, Ministry of Education, Jinan 250100, China. E-mail: jhao@sdu.edu.cn; Fax: +86-531-88564750*
[b] *Physikalische Chemie I, Bayreuth Universität, D-95440, Germany*

† Electronic supplementary information (ESI) available. See DOI: 10.1039/c9nj04252k

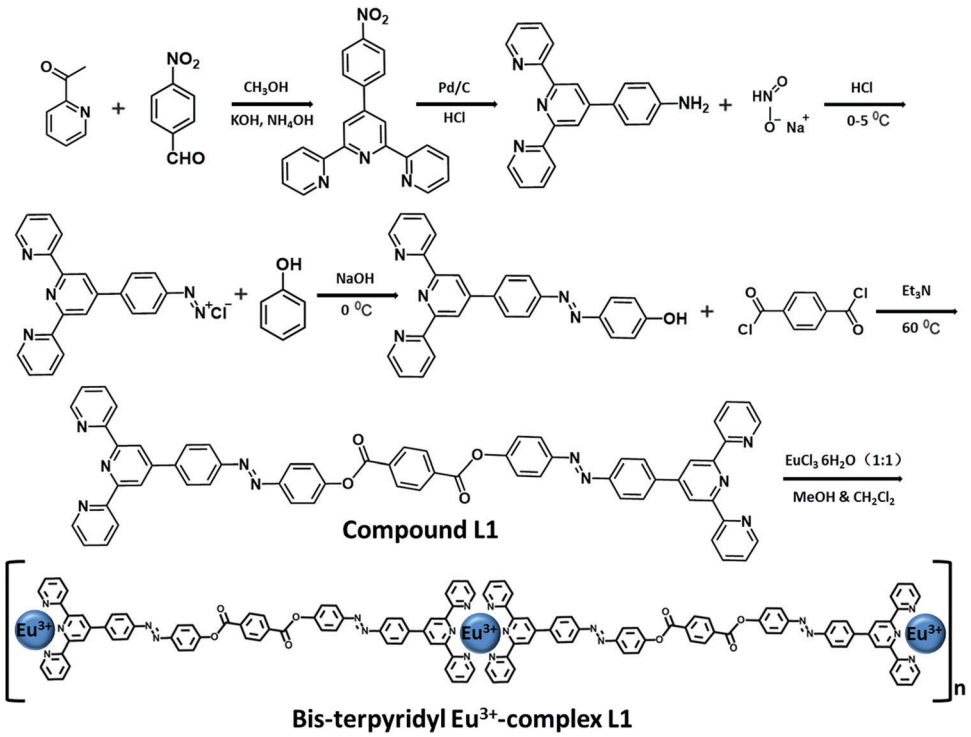

Scheme 1 Synthetic route of **compound L1** and **bis-terpyridyl Eu^{3+}-complex L1**.

was clearly demonstrated. Our results could be significant for synthesizing fluorescent molecules and controlling the aggregation behavior of responsive terpyridyl-metal-coordinated luminescent materials. **Compound L1** and **bis-terpyridyl Eu^{3+}-complex L1** are shown in Scheme 1 along with the synthetic route.

2. Experimental

2.1 Chemicals and materials

2-Acetylpyridine (98%, M_w = 121.05) and 4-nitrobenzaldehyde (99%, M_w = 151.03) were purchased from J&K Chemical Ltd (Shanghai, China). Phenol (99%, M_w = 94.11), paraphthaloyl chloride (98%, M_w = 203.02) and $EuCl_3{\cdot}6H_2O$ (98%, M_w = 366.32) were purchased from TCI Development Co., Ltd (Shanghai, China). Ethyl alcohol (99%, analytical reagent, AR), dichloromethane (99%, AR), methyl alcohol (99%, AR), chloroform (99%, AR) and acetone (99%, AR) were purchased from Kermel Reagent Co., Ltd (Tianjin, China). Inorganic alkalis and salts such as NaOH, $NaNO_2$ and anhydrous Na_2SO_4 were obtained from China Sinopharm Chemical Reagent Co., Ltd (Shanghai, China). All chemicals were received without further purification. The water used in all experiments was purified three times with a UPH-IV ultrapure water apparatus (China) and had a resistivity greater than 18.25 MΩ cm.

2.2 Synthesis

2.2.1 Synthesis of 4′-(4-nitrophenyl)-2,2′:6′,2″-terpyridine. 4-Nitrobenzaldehyde (3.17 g, 21 mmol) and 2-acetylpyridine (5 g, 41.5 mmol) were dissolved in methanol (170 mL) with vigorous stirring till they dissolved completely. A mixture of NH_4OH (160 mL) and KOH solution (15%, 15 mL) was injected in the above solution. The reaction was incubated at room temperature for 3 days. The precipitates were collected, washed with cold methanol 3 times, and dissolved in ethyl acetate. The organic phase was extracted with $NaHCO_3$ (1 wt%) solution and dried with anhydrous Na_2SO_4. After the removal of the organic solvent by rotary evaporating, the brown product was recrystallized twice with ethyl alcohol, resulting in the product (yield: 30%): m.p. 210–211 °C, ^{1}H NMR (400 MHz, $CDCl_3$), δ(ppm): 8.74 (m, 4H), 8.69 (d, J = 7.95 Hz, 2H), 8.37 (d, J = 8.57 Hz, 2H), 8.05 (d, J = 8.54 Hz, 2H), 7.91 (t, J = 7.73 Hz, 2H), 7.38 (m, 2H).

2.2.2. Synthesis of 4′-(4-aminophenyl)-2,2′:6′,2″-terpyridine. This reaction was conducted under nitrogen (N_2) protection. 4′-(4-Nitrophenyl)-2,2′:6′,2″-terpyridine (1.0 g, 2.82 mmol) and 10% Pb/C (100 mg) were dissolved in ethanol (200 mL) and stirred for 3 h. Celitepad was used to filter off the catalyst. After washing with ethanol (100 mL), the solvent was removed under reduced pressure. The remaining solid was freeze-dried from distilled water (10 mL) to give a pure beige product (yield: 94%): m.p. 253–254 °C, ^{1}H NMR (400 MHz, DMSO-d_6) δ (ppm): 5.59 (s, 2H), 6.73 (d, $3J$ = 8.72 Hz, 2H), 7.50 (ddd, $3J$ = 7.45 Hz, $3J$ = 4.8 Hz, $4J$ = 1.13 Hz), 7.66 (d, $3J$ = 8.59 Hz), 8.02 (td, $3J$ = 7.71 Hz, $4J$ = 1.77 Hz), 8.62 (s, 2H), 8.65 (dt, $3J$ = 7.96 Hz, $4J$ = 1.14 Hz),8.74 (ddd, $3J$ = 4.8 Hz, $4J$ = 1.77 Hz, $5J$ = 0.89 Hz).

2.2.3. Synthesis of 4-((4′-2,2′:6′,2″-terpyridine)phenylazo) phenol. 4′-(4-Aminophenyl)-2,2′:6′,2″-terpyridine (200 mg, 0.62 mmol) was dissolved in HCl (37%, 500 μL) under sonication. $NaNO_2$ solution (20 mg mL^{-1}) was added dropwise into the reaction mixture at T = 0 °C until it made the potassium

iodide-starch test paper turn blue. The obtained diazonium salt solution was stirred for 1 h and transferred into 10 mL aqueous solution of phenol (58.1 mg, 0.617 mmol) and NaOH (170 mg, 4.25 mmol). The reaction was maintained for another 12 h at room temperature (~25 °C). Red precipitate was collected by filtration and washed with brine and distilled water for 3 times to obtain the pure product (yield: 81%): ^{1}H NMR (400 MHz, DMSO-d_6) δ (ppm): 10.33 (s, 1H), 8.81 (m, 4H), 8.74 (d, J = 8.00 Hz, 2H), 8.16 (d, J = 8.00 Hz, 2H), 8.11 (td, 3J = 7.75 Hz, 4J = 1.80 Hz, 2H), 8.03 (d, J = 7.75 Hz, 2H), 7.88 (d, J = 8.00 Hz, 2H), 7.59 (ddd, 3J = 7.45 Hz, 3J = 4.5 Hz, 4J = 1.20 Hz, 2H), 6.99 (d, J = 7.80 Hz, 2H).

2.2.4. Synthesis of compound L1. All glass bottles were dried before using. 4-((4′-2,2′:6′,2″-terpyridine) phenylazo) phenol (188 mg, 0.44 mmol) was suspended in 90 mL dried dichloromethane and stirred for 5 min in nitrogen atmosphere with reflux condensation. Triethylamine (88.7 mg, 0.88 mmol, dried with calcium hydride) dissolved in 10 mL dichloromethane was added into the mixture. After being stirred for 10 min, 50 mL dichloromethane solution of terephthaloyl chloride (44.5 mg, 0.22 mmol) was added dropwise into the reaction (turbid reaction liquid turned into clear solution). After being maintained at T = 60 °C in an oil bath for 48 h, the mixture was rotary evaporated to remove the solvent. The remaining precipitate was dissolved in dichloromethane and extracted by NaCl solution and distilled water for 3 times, respectively. The organic phase obtained was dried with anhydrous $NaSO_4$ for 20 min and recrystallized by hexane for 2 times to give yellowish-brown powder (yield: 92%). The ^{1}H NMR (400 MHz, DMSO-d_6) spectrum of **compound L1** is shown in Fig. 1a.

2.2.5. Synthesis of bis-terpyridyl Eu^{3+}-complex L1. **Compound L1** (20 mg, 0.02 mmol) and $EuCl_3{\cdot}6H_2O$ (7.41 mg, 0.02 mmol) were added into a mixed solvent of dichloromethane and methanol (v : v = 1 : 1). The reaction temperature was maintained at T = 50 °C overnight with reflux condensation. The reaction mixture was centrifuged (8000 rpm, 20 min) and the bronzing precipitate was collected. After washing 3 times with methanol, the precipitate was dried to obtain the pure product. The ^{1}H NMR (400 MHz, DMSO-d_6) spectrum of **bis-terpyridyl Eu^{3+}-complex L1** is shown in Fig. 1a.

2.2.6. Synthesis of bis-terpyridyl Eu^{3+}-complex L2. **Compound L1** (20 mg, 0.02 mmol) and $EuCl_3{\cdot}6H_2O$ (16.7 mg, 0.045 mmol) were weighed and the same reaction procedures described above were carried out. The product was coordinated with **compound L2** in the mixed solvent of dichloromethane and methanol (v : v = 1 : 1). **Compound L2** was synthesized, as shown in Scheme S1 in the ESI.† After centrifugal purification, **bis-terpyridyl Eu^{3+}-complex L2** was collected with the appearance of brownish black powder.

2.3 Characterizations

The precipitates (2 mg) of **bis-terpyridyl Eu^{3+}-complex L1** or **bis-terpyridyl Eu^{3+}-complex L2** were dissolved in 10 mL methanol. The solution was stirred and sealed before detection. Fluorescence spectra were collected on a Hitachi F-7000 steady-state and time-resolved fluorescence spectrofluorometer. Morphologies of the aggregates were observed on a JEOLJEM-1400 transmission electron microscope and a Hitachi S-4800 field emission scanning electron microscope. Topologies of the aggregates were measured

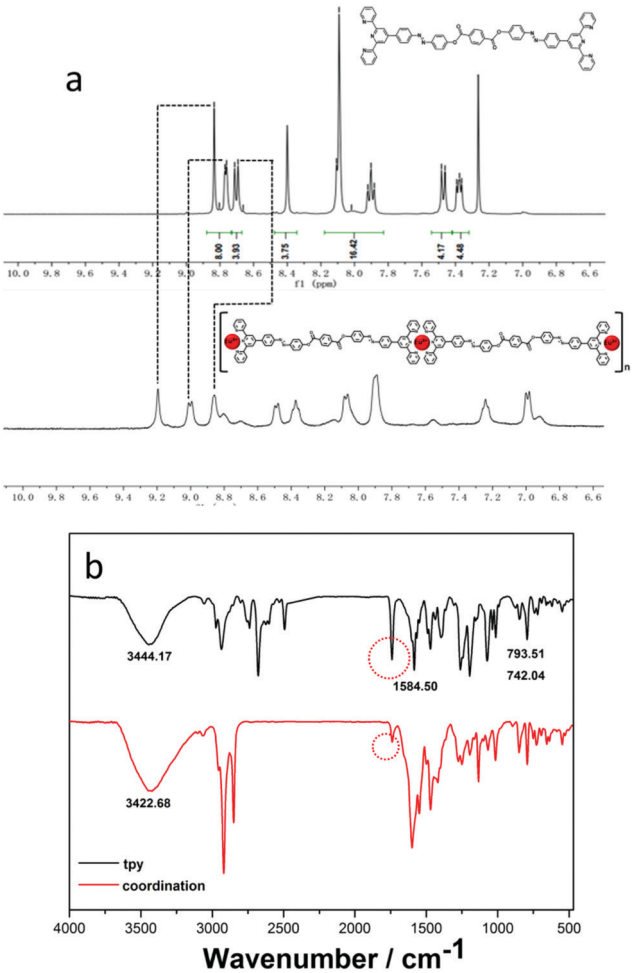

Fig. 1 (a) ^{1}H NMR spectra (400 MHz, DMSO-d_6) of **compound L1** and **bis-terpyridyl Eu^{3+}-complex L1**. Low field shift of the pyridine protons from 8.66–8.83 ppm to 8.90–9.22 ppm was observed. (b) Infrared spectra of **compound L1** and **bis-terpyridyl Eu^{3+}-complex L1**. The wavenumber shifted from 1584.50 cm^{-1} of **compound L1** to 1599.22 cm^{-1} of **bis-terpyridyl Eu^{3+}-complex L1**.

with a VeecoNanosope IIIa atomic force microscope operating in the tapping mode. Infrared spectra were recorded on a Bruker Optics VERTEX-70/70v FT-IR spectrometer within the range from 500 cm^{-1} to 4000 cm^{-1}. The substrates (glass, silicon wafer) used in our experiments were cleaned in acetone and distilled water under sonication, respectively.

To prepare dust-free solutions for DLS measurements, all sample solutions were filtered directly into dust-free light scattering cells through different Millipore non-sterile membrane filters (0.22 μm and 0.45 μm) depending on the concentrations and the sizes of the aggregates. The light-scattering cells were rinsed inside and outside with distilled (dust-free) acetone to ensure a dust-free condition before use. A standard laboratory-built laser light scattering spectrometer equipped with a Coherent Radiation 200 mW diode pumped solid-state (DPSS) 532 laser operating at 532 nm and a Brookhaven Instruments (BI-9000AT) correlator was used for the DLS measurements. The spectrometer is capable of making measurements of both the angular dependence of absolute

integrated scattered intensity over a scattering angular range from 20° to 140° and of intensity–intensity digital photon correlation over a similar angular range (DLS and depolarized DLS). About 2–3 mL of sample solutions was transferred into a special dust-free light scattering cell for light scattering measurements. The scattering cells were held in a brass thermostat block filled with refractive index-matching silicone oil. The temperature was controlled to within ±0.05 °C. DLS measures the intensity–intensity time correlation function $G^{(2)}(\Gamma)$ in the self-beating mode by means of a multi-channel (BI-9000) digital correlator. $G^{(2)}(\Gamma)$ can be related to the electric field time correlation function $g^{(1)}(\tau)$:

$$G^{(2)}(\Gamma) = A(1 + b|g^{(1)}(\tau)|^2) \quad (1)$$

Here, A and b are the background (baseline) and a coherence factor (a parameter depending on the detection coherence), respectively. The electric field time correlation function, $g^{(1)}(\tau)$, was analyzed by the constrained regularized CONTIN method[20] to yield information on the distribution $G(\Gamma)$ of the characteristic line width (Γ) from

$$|g^{(1)}(\tau)| = \int_0^\infty G(\Gamma)\exp(-\Gamma\tau)\mathrm{d}\Gamma \quad (2)$$

The first and second moments of $G(\Gamma)$ are $\langle\Gamma\rangle = \int_0^\infty \Gamma G(\Gamma)\mathrm{d}\Gamma$ and $\mu_2 = \int_0^\infty (\Gamma - \langle\Gamma\rangle)^2 G(\Gamma)\mathrm{d}\Gamma$, respectively. The value of $\mu_2/\langle\Gamma\rangle^2$ is a measure of the particle polydispersity. If the relaxation is diffusive, Γ can be related to the average apparent diffusion coefficient (D_{app}):

$$D_{app}(1 + k_d c)(1 + f\langle R_g^2\rangle q^2) = \Gamma/q^2 \quad (3)$$

Here, k_d is the diffusive second virial coefficient, R_g is the radius of gyration, q is the magnitude of the scattering wave vector, and f is a dimensionless factor related to hydrodynamic draining, internal motion, polydispersity, and solvent quality. If the average apparent diffusion coefficient (D_{app}) is known, the apparent hydrodynamic radius, R_h, can be obtained *via* the Stokes–Einstein equation:

$$R_h = k_B T/6\pi\eta D_{app} \quad (4)$$

Here, k_B is the Boltzmann constant, and η is the viscosity of the solvent at temperature T. From DLS measurements, we can obtain the particle-size distribution in solution from a plot of $\Gamma\cdot G(\Gamma)$ *vs.* R_h, with $\Gamma\cdot G(\Gamma)$ being proportional to the scattered intensity of ith particles having an apparent hydrodynamic radius R_h. DLS measurements were performed at finite concentrations, where inter-particle interactions have been neglected.

3 Results and discussion

3.1 Synthesis of bis-terpyridyl Eu^{3+}-complex L1

A long-chain ligand of the coordination **compound L1**, as shown in Scheme 1, was synthesized. After being coordinated with $EuCl_3\cdot 6H_2O$, the fabricated **bis-terpyridyl Eu^{3+}-complex L1** was dissolved in methanol and exhibited prominent UV- responsive emission enhancement. **Compound L1** with azobenzene was employed as allosteric groups to offer UV-responsive isomerization. With the coordination link of each terpyridine group, the configuration change of a mono molecule was extended to the transformation of the assembling microstructures.

Fig. 2 Photographs of the **bis-terpyridyl Eu^{3+}-complex L1** methanol solution at c = 0.2 mg mL^{-1} with (right) and without (left) UV radiation.

Tpy-NH_2 was first synthesized using a previously reported method.[21,22] The resulting product was conjugated with phenol by the diazotization coupling reaction to introduce azobenzene groups. The chemical structure of **compound L1** was characterized by ^{1}H-NMR spectra shown in Fig. 1a and MALDI-TOF-MS results shown in Fig. S1 in the ESI.† The sharp peaks from 8.66 ppm to 8.83 ppm in Fig. 1a can be ascribed to the protons in pyridine. The mass spectrum of **compound L1** in Fig. S1 in the ESI† shows the presence of a molecular ion peak with m/z = 989.86, demonstrating the successful formation of the product. Another compound was assigned to be **compound L2**, as shown in Scheme S1 in the ESI,† and its ^{1}H NMR spectrum is shown in Fig. S2 in the ESI.†

The successful preparation of **bis-terpyridyl Eu^{3+}-complex L1** was also investigated by ^{1}H NMR and infrared spectroscopy. As shown in Fig. 1a, the characteristic peaks of the protons in pyridine yield a low field shift from 8.66–8.83 ppm to 8.90–9.22 ppm due to the lower electron density of pyridine after coordination. Meanwhile, the sharp peaks of protons change into a broad shape, which is commonly observed after the dynamic inhibition of the protons.[23] As shown in Fig. 1b, the C–N characteristic peak for pyridine (1584.50 cm^{-1}) weakened after coordination, which was due to the N-metal interaction in **bis-terpyridyl Eu^{3+}-complex L1**.[24] The presence of europium within **bis-terpyridyl Eu^{3+}-complex L1** was demonstrated by X-ray photoelectronic spectroscopy (XPS). The spectrum shown in Fig. S3 in the ESI† exhibits the presence of C 1s, O 1s, N 1s and Eu 3d. The deconvolution of the N 1s signal generates two singlets. The singlet at 389.5 eV comes from the N–C units; the singlet at 399.1 eV is derived from the N–Eu units, which indicates the complexation between Eu^{3+} and terpyridyl groups (Fig. S3b, ESI†).

After centrifugal purification, **bis-terpyridyl Eu^{3+}-complex L1** was suspended in methanol with a final concentration of 0.2 mg mL^{-1}. As shown in Fig. 2, the methanol solution of **bis-terpyridyl Eu^{3+}-complex L1** exhibits the yellowish-brown color of the azobenzene chromophore.

3.2 Excitation and emission spectra of bis-terpyridyl Eu^{3+}-complex L1 and fluorescence variations under ultraviolet radiation

At λ = 365 nm ultraviolet radiation, indigo fluorescence was observed with the naked eye. The excitation and emission

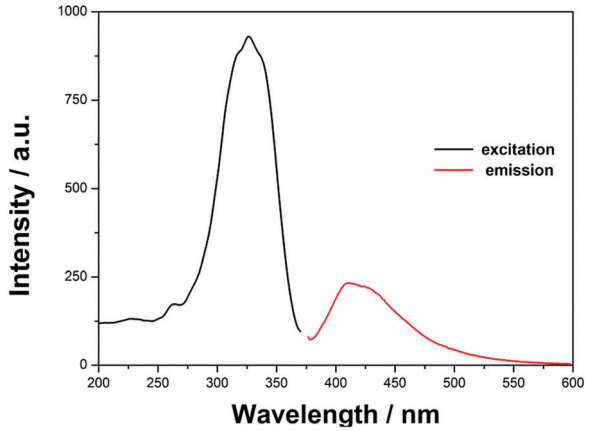

Fig. 3 Excitation and emission spectra of **bis-terpyridyl Eu^{3+}-complex L1** in methanol solution.

spectra of the fluorescent solution were measured. Fig. 3 shows an excitation peak at λ = 326 nm and a relatively weak emission peak ranging from 380 nm to 575 nm. Interestingly, there is no overlap between its excitation and emission curves. It has been demonstrated that an overlapped area between excitation and emission may lead to non-radiative transformation from the ground state to the excited state. The aggregation fluorescence can be quenched to decrease the fluorescence efficiency, which is the so-called aggregation-caused quenching (ACQ) effect.[10] We believe that the separation of excitation and emission can decrease the influence of the ACQ effect.

Azobenzene molecules exhibit *trans–cis* isomerization under UV radiation.[25–30] To investigate the fluorescence variations introduced by a configuration change, 1 mL solution of **bis-terpyridyl Eu^{3+}-complex L1** in methanol was exposed under a UV mercury lamp with a filter of 365 nm, as shown in Fig. 4a. After being exposed to ultraviolet radiation for 120 min, the solution of **compound L1** in methanol exhibited prominent fluorescence enhancement, which was visible by the naked eye (Fig. 4b). The fluorescence quantum yield of the solution increased from 2.9% to 10.6% (Fig. S4 in the ESI†) and the fluorescence lifetime increased from 5.85 ns to 9.87 ns (Fig. S5 in the ESI†), suggesting the enhanced photoluminescence capability of the material. The excitation spectra of the fluorescent solutions before/after UV irradiation were measured. As shown in Fig. 4c, a significant redshift from 326 nm (black line) to 350 nm (red line) is observed, confirming that the configuration transforms from *trans* to *cis*.

The continuous fluorescence enhancement was investigated after the solutions were exposed to UV radiation for different time periods. The emission spectra of the solutions after radiation for 0, 5, 15, 30, 60, and 120 min are shown in Fig. 5. It can be observed from Fig. 5a that the blank group without UV exposure exhibits a weak emission intensity of 232 (a.u.). With the exposure time continuously increasing, the emission intensity of the fluorescent solution enhances prominently (Fig. 5b). A redshift was obviously observed after 60 min. The solution fluorescence (intensity enhancement and emission shift) became stable after 120 min radiation. As shown in Fig. 5c, the emission intensity after 120 min is an order of magnitude higher (about 5 times) than that at 0 min.

The fluorescence variations of **bis-terpyridyl Eu^{3+}-complex L1** in methanol solutions before and after ultraviolet radiation are listed in Table 1. After 120 minutes of UV radiation, the excitation peak shifted from 326 nm to 350 nm and the emission peak shifted from 411 nm to 438 nm. The emission intensity increased by about 5 times the initial value. The corresponding quantum yield increased from 2.9% to 10.6% and the fluorescence lifetime increased from 5.85 ns to 9.87 ns.

3.3 Self-assembly of bis-terpyridyl Eu^{3+}-complex

The *trans–cis* isomerization of azobenzene molecules resulted in the configuration variation of **compound L1** (Fig. 4a), which subsequently changed the structure of the aggregates *via* coordination. In order to investigate the intramolecular mechanism of the UV-responsive fluorescence enhancement, the influence of the monomers and aggregates was separately investigated.

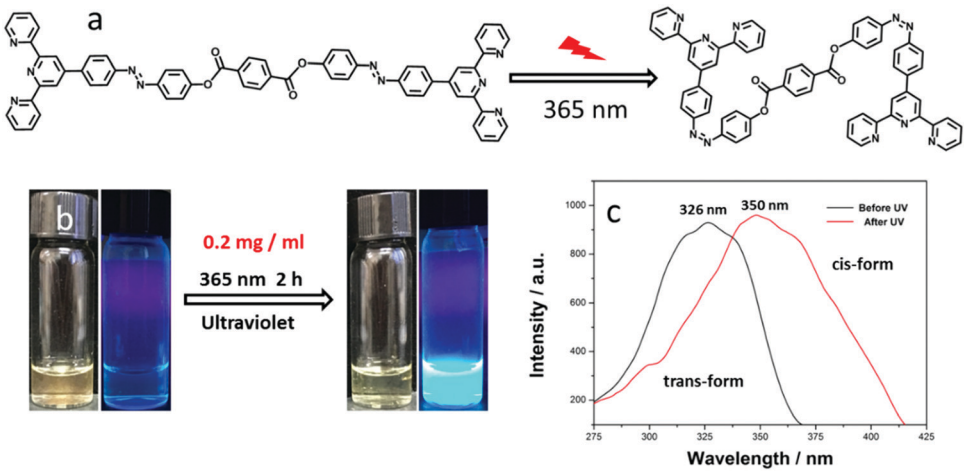

Fig. 4 (a) Schematic illustration of *trans–cis* transformation of **compound L1**. (b) Images of the coordination solution before/after UV irradiation. (c) Excitation spectra of the fluorescent solution before (black) and after (red) UV irradiation, where a red shift from 326 nm to 350 nm is observed.

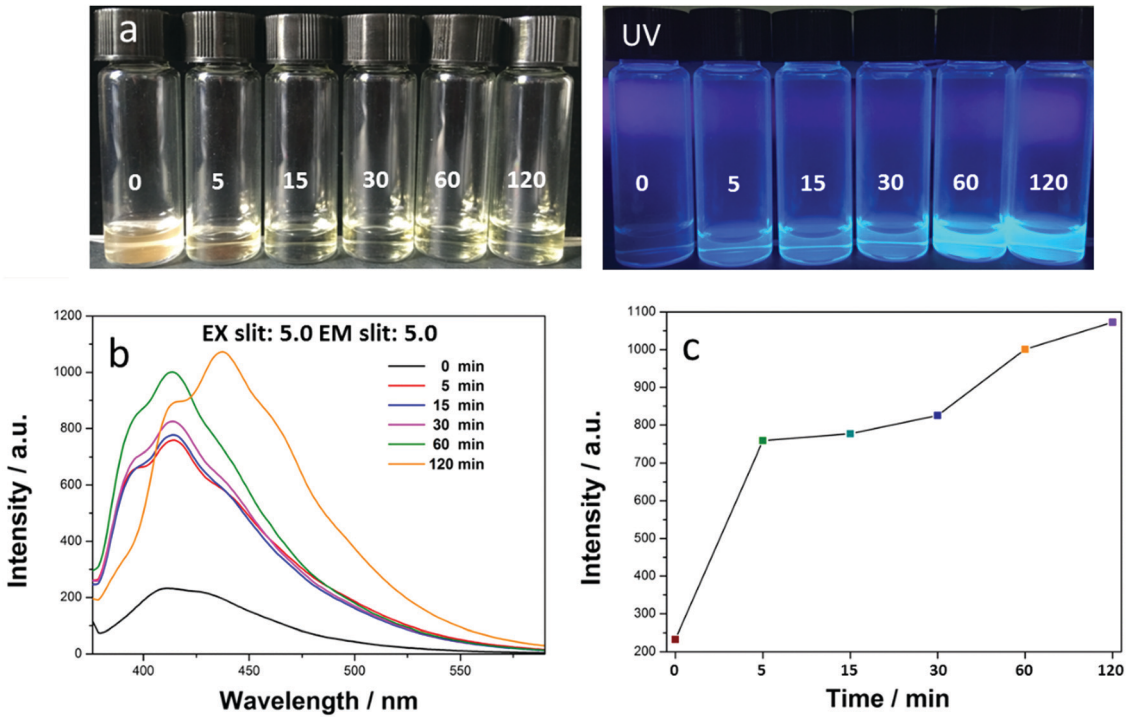

Fig. 5 (a) Photographs of the solution (0.2 mg mL^{-1}) before and after UV exposure of 0, 5, 15, 30, 60, 120 min. (b) Emission spectra of the solution after radiation of 0 (black), 5 (red), 15 (blue), 30 (purple), 60 (green), 120 (orange) min. (c) Emission intensity of the fluorescent solution after UV exposure for 0, 5, 15, 30, 60, 120 min.

Table 1 Variations of fluorescence before and after UV exposure

	0 min	120 min
Excitation peak/nm	326	350
Emission peak/nm	411	438
Emission intensity/a. u.	232.6	1072.6
Quantum yield/%	2.9	10.6
Fluorescence lifetime/ns	5.85	9.87

We contrastively synthesized **bis-terpyridyl Eu^{3+}-complex L2** with similar equivalents of N and O atoms (contains n-electrons, easy to form hydrogen bonds). Based on the synthesis route presented in Scheme S1 in the ESI,† **compound L2** was obtained through a condensation reaction of 4′-(4-aminophenyl)-2,2′:6′,2″-terpyridine and acetic acid. Stepwise assembly was subsequently employed to obtain **bis-terpyridyl Eu^{3+}-complex L2** (Scheme S1 in the ESI†). This coordination reserved the main structure of azobenzene and eliminated the long-chain connection of the aggregates.

After being dissolved in methanol with the same concentration of 0.2 mg mL^{-1}, the morphology of **bis-terpyridyl Eu^{3+}-complex L2** was investigated. As expected, there were no specific aggregates observed under a scanning electron microscope (Fig. S6 in the ESI†). The emission spectra of the fluorescent solutions treated at λ = 365 nm for different times (0, 5, 10, 15, 30, 60, and 120 min) were measured (Fig. S7 in the ESI†). On increasing the UV exposure times, no significant change in the emission peak (410 nm) occurred. As shown in Fig. S7b in the ESI,† the statistic emission intensity of the samples indicates no obvious variation. Therefore, the UV-responsive isomerization of the monomers does not contribute to the fluorescence enhancement of the solution.

Based on the above results, the morphology changes in the aggregation behavior of **bis-terpyridyl Eu^{3+}-complex L1** were also studied. Before UV exposure, 10 μL of **bis-terpyridyl Eu^{3+}-complex L1** in ethanol was dropped on a silicon wafer and copper grids for performing SEM, AFM and TEM. Optical and inverted fluorescence microscopy characterizations were also carried out to offer comparison (Fig. 6). The optical microscopy (Fig. 6a), inverted fluorescence microscopy (Fig. 6b), and SEM images (Fig. 6c) reveal that large aggregates assemble by the clusters of nanoparticles with diameters around 500 nm. To investigate the mono-dispersed units of the aggregates, 10 μL fluorescent liquid was spin-coated at the substrate surface with a rotation speed of 4000 rpm. In the central area, mono-dispersed units can be observed. The typical SEM image clearly shows dispersive nanoparticles with diameters from 20 to 30 nm (Fig. 6f), and this was consistent with the AFM (Fig. 6d) and TEM (Fig. 6e) images. Considering the *trans* to *cis* transformation of **compound L1**, confirmed by Fig. 4a and c, these nanosphere-shaped aggregates assembled by the mono-dispersed units of **bis-terpyridyl Eu^{3+}-complex L1**, which could be compared with **bis-terpyridyl Eu^{3+}-complex L2**, were speculated to be a relatively loose assembly of long-chain coordination because enough space should exist for the transition from the *trans* to *cis* isomerization of azobenzene with UV exposure. After UV exposure for 120 min, the microstructure of the aggregates became packed micron sheets, as shown in Fig. 6g and h.

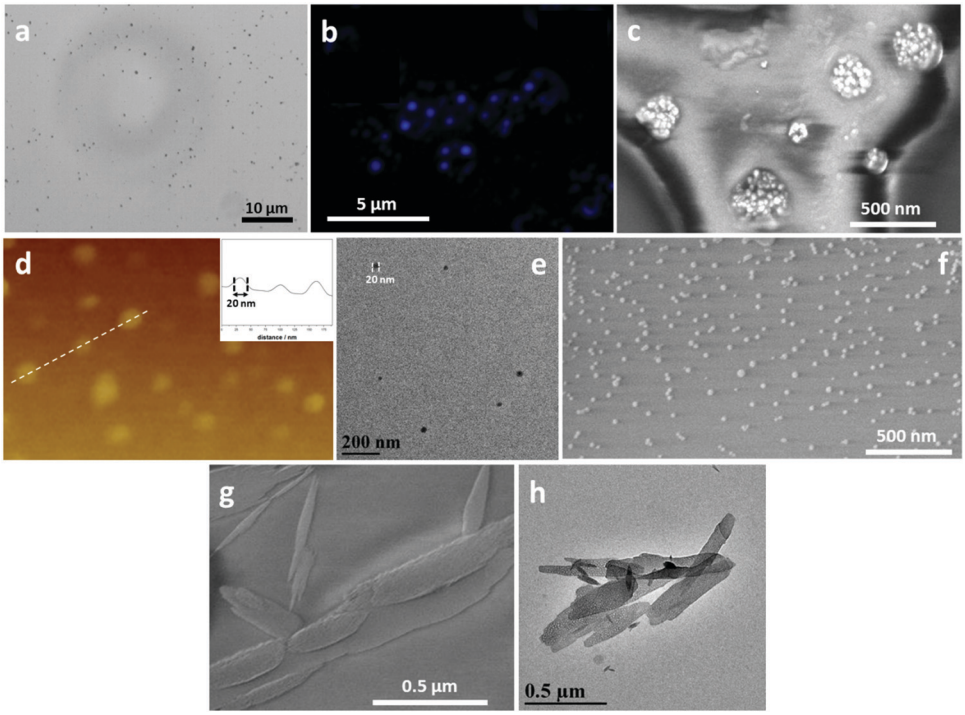

Fig. 6 (a) Optical microscopy, (b) fluorescence microscopy and (c) SEM images of **bis-terpyridyl Eu^{3+}-complex L1** before UV radiation. After suspended coating on substrates with rotation speed of 4000 rpm, the mono-dispersed aggregates can be observed in (d) AFM, (e) TEM and (f) SEM images as nanoparticles with diameters from 20 to 30 nm. After 120 minutes of UV radiation, the micron sheet-shaped aggregates can be observed in (g) SEM and (h) TEM images.

AFM measurements in the tapping mode were employed to calculate the thickness of each sheet, and Gaussian simulations for the lowest energy state of **compound L1** in methanol were also performed. As shown in Fig. 7a and b, the monolayer height of one sheet is 0.9 nm, which corresponds to the theoretical length of the terpyridyl head group (9.4 Å). According to the measured result, there are reasons to believe that these stacked micron sheets are closely packed assemblies of **bis-terpyridyl Eu^{3+}-complex L1** with *cis*-isomerized azobenzene groups. To prove this speculation, the UV-treated solution was placed in visible light for 30 days and incubated at 60 °C in a water bath for 12 h. As expected, there was no change in its fluorescence performance and aggregates, indicating that a tight steric hindrance between each sheet inhibited the *cis* to *trans* recovery of **compound L1**.

Gaussian simulations for the lowest energy state of **compound L1** in methanol were performed. As shown in Fig. 7c and d, the theoretical thickness of the monolayer terpyridyl head group is 9.4 Å. The AFM calculations of the UV-treated sample demonstrated that the distance between two packed layers was 0.9 nm, which was consistent with the simulated thickness.

Based on our dynamic laser light scattering (DLS) data of the CONTIN analysis for a typical sample solution of 0.2 mg mL^{-1} **bis-terpyridyl Eu^{3+}-complex L1** before and after UV exposure, Fig. 8a shows plots of the intensity contribution function $\Gamma_i \cdot G(\Gamma)$ *vs.* the apparent hydrodynamic radius (R_h) for the **bis-terpyridyl Eu^{3+}-complex L1** methanol solutions at different scattering angles as indicated. The size distribution of the aggregates of **bis-terpyridyl Eu^{3+}-complex L1** before UV exposure exhibited only a unimodal peak with an average hydrodynamic radius $\langle R_h \rangle$ of about 485.4 nm and polydispersity of $\mu_2/\langle\Gamma\rangle^2 \approx 0.19$. The size distributions of the three scattering angles (30°, 60° and 90°) did not indicate apparent angular dependence. The lack of apparent angular dependence could indicate that impermeable spherical shells, *i.e.*, hollow spheres in the limit of infinitely thin wall thickness existed as nanospheres.[31] However, the obtained size diameters of the dispersive nanospheres from the SEM and TEM images were in the range from 20 to 30 nm, indicating that large aggregates could exist. The TEM images (Fig. 6) clearly demonstrate the presence of large aggregates with the average sizes between 300 and 600 nm, which are consistent with the DLS measurements. The large aggregates were assembled by the dispersive nanospheres with diameters from 20 to 30 nm (Fig. 6a). After the sample solution was exposed to UV light for 120 min, DLS measurements were obtained. As shown in Fig. 8b, two or three peaks can be identified at different scattering angles (30° and 90°) with different sizes, *i.e.*, ~15 nm, ~40 nm and 2000 nm at θ = 90° and 90 nm and 1500 nm at θ = 30°, which have apparent angular dependence. The DLS measurements could indicate that different assembled structures were formed after UV exposure, which contained closely packed nanosheets with different sizes, as obtained from Fig. 6d and e.

Based on the above characterizations of the TEM, SEM and DLS data, a schematic of the fluorescence enhancement is shown in Fig. 9. Before UV exposure, **compound L1** appeared

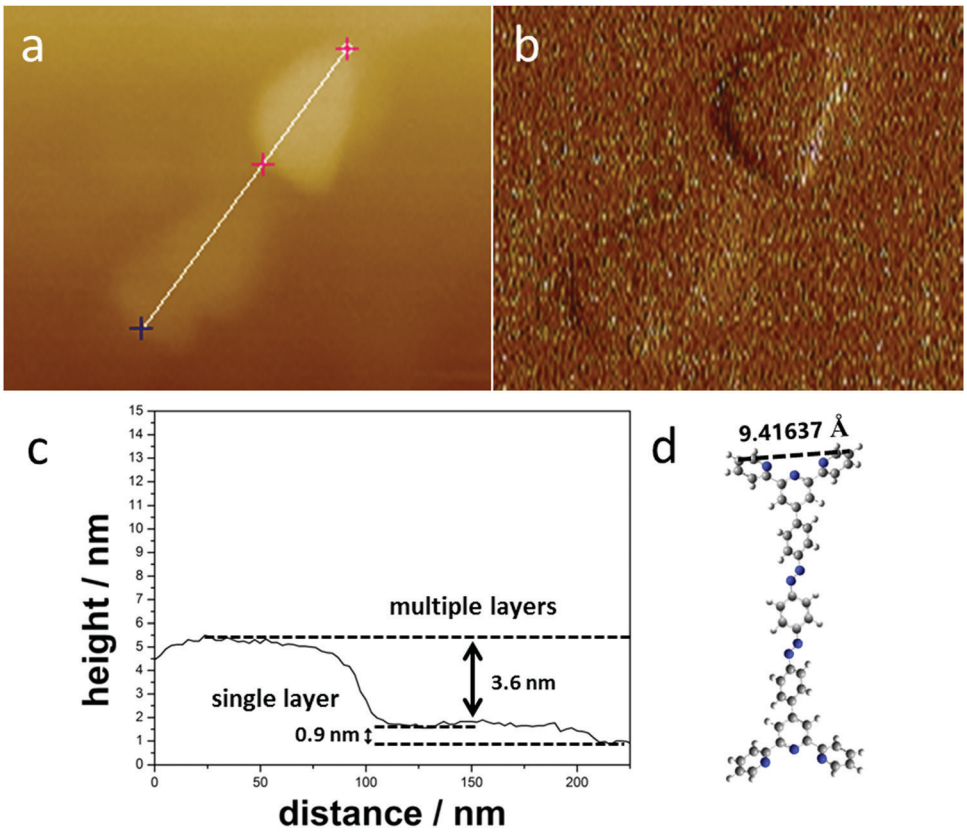

Fig. 7 (a) AFM image, (b) imaging mode and (c) topological measurement of the coordinated aggregation after UV radiation. (d) Gaussian simulation of **compound L1** in methanol with monomolecular thickness of 0.9 nm.

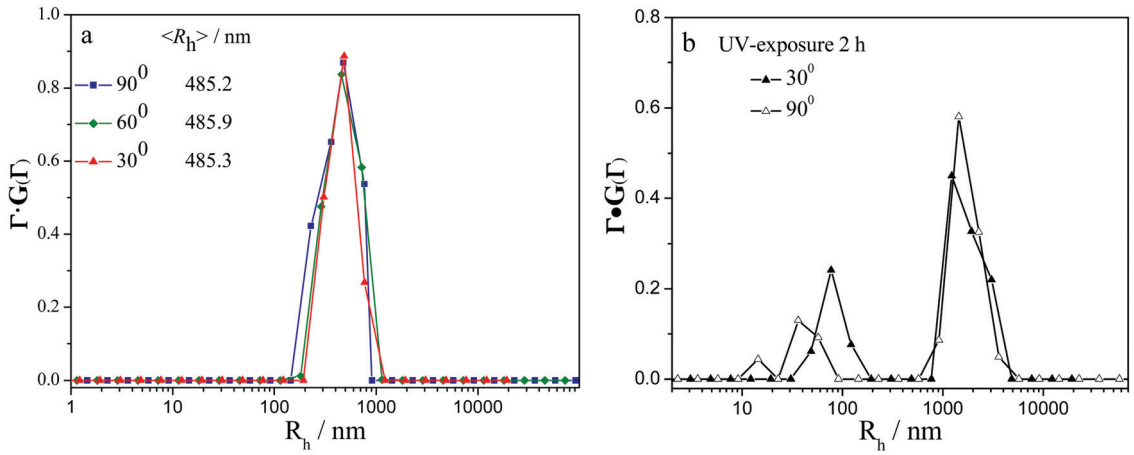

Fig. 8 Dynamic laser light scattering (DLS) measurements and TEM image of the aggregates of **bis-terpyridyl Eu^{3+} complex L1**. DLS data of the coordinated aggregates (a) with the size of 500 nm, which did not indicate apparent angular dependence before UV radiation. DLS data of coordinated aggregates with different peaks, which indicated apparent angular dependence (b) after UV radiation.

mainly in *trans* configuration, where coordinated aggregates existed in the form of nanoparticles with diameters from 20 to 30 nm. Due to the high surface energy of the nanoparticles, they tended to aggregate as impermeable spheres with an average diameter of 485.4 nm. This loosely packed structure offered enough space for molecular isomerization. On increasing the time of UV radiation, the configuration of **compound L1** twisted from *trans* to *cis*. The isomerization of the **compound L1** molecules soon expanded to the whole structure *via* Eu^{3+}-introduced coordinated connection, which transformed the aggregates to closely packed micron sheets with monolayer thickness of 0.9 nm (the width of a terpyridyl group). We speculate that the steric hindrance between each sheet inhibits the intramolecular rotation of the C–C bond and increases the area of π-conjugated fluorophores. Meanwhile, intermolecular nonradiative energy transfer is hard to generate between each sheet because there is nearly no overlap

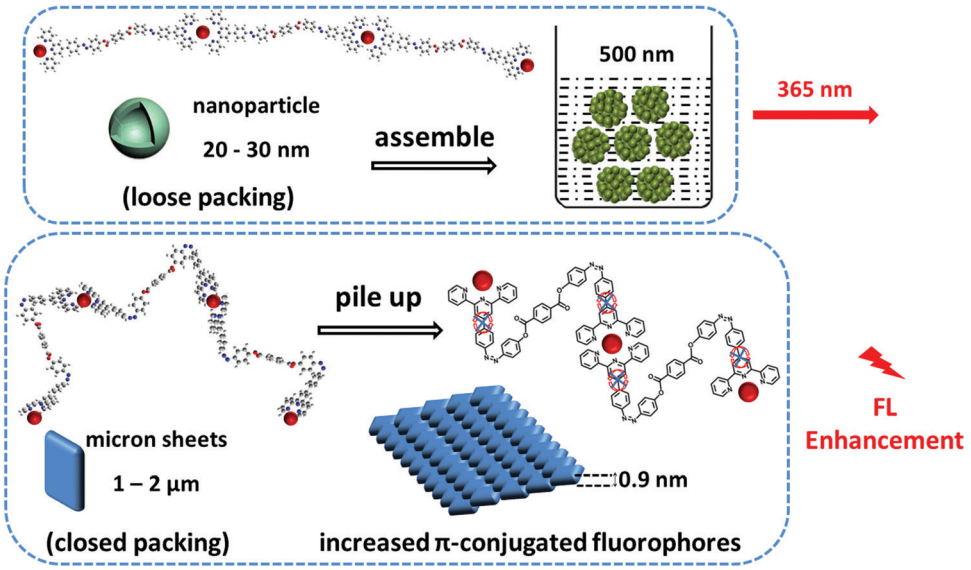

Fig. 9 Schematic illustration of the speculated structural transformation from nanoparticles to micron sheets introduced by the *trans–cis* isomerization of **bis-terpyridyl Eu^{3+}-complex L1** and the mechanism of fluorescence enhancement.

between the coordination's excitation and emission curves. With the influence of both factors, the fluorescence performance of **bis-terpyridyl Eu^{3+}-complex L1** exhibited apparent enhancement.

4. Conclusions

In conclusion, we synthesized a luminescent molecule **compound L1** with an azobenzene-functionalized chain between two terpyridine ligands by the diazotization coupling reaction. Eu^{3+} was employed to form long-chain coordinated **bis-terpyridyl Eu^{3+}-complex L1**. After being dissolved in methanol and exposed to UV light, the fluorescent solution exhibited significant emission enhancement with separated excitation and emission. The morphological structure of the coordination complex showed a prominent transformation from clustered nanoparticles to micron sheets. The thickness of the monolayer micron sheet from AFM measurements was consistent with the Gaussian simulative width of a terpyridyl head group, indicating the closed packing of the aggregates. It is speculated that the transformation from loosely packed nanoparticles to closed packed micron sheets introduced by the *trans–cis* isomerization causes the emission enhancement. This work is expected to facilitate the developments of metal–organic molecules and provides a novel strategy for responsive fluorescent materials.

Conflicts of interest

There are no conflicts to declare.

Acknowledgements

This work was funded by the National Natural Science Foundation of China (Grant No. 21420102006), the Natural Science Foundation of Shandong Province (ZR2018ZA0547).

Notes and references

1 K. Pu and B. Liu, *Adv. Funct. Mater.*, 2011, **21**, 3408–3423.
2 J. Kim, K. Park, H. Y. Nam, S. Lee, K. Kim and I. C. Kwon, *Prog. Polym. Sci.*, 2007, **32**, 1031–1053.
3 L. Yuan, W. Lin, S. Zhao, W. Gao, B. Chen, L. He and S. Zhu, *J. Am. Chem. Soc.*, 2012, **134**, 13510–13523.
4 L. Yuan, W. Lin, Y. Xie, B. Chen and S. Zhu, *J. Am. Chem. Soc.*, 2012, **134**, 1305–1315.
5 K. C. Ko, J. Wu, H. J. Kim, P. S. Kwon, J. W. Kim, R. A. Bartsch, J. Y. Lee and J. S. Kim, *Chem. Commun.*, 2011, **47**, 3165–3167.
6 T. D. Ashton, K. A. Jolliffe and M. Pfeffer, *Chem. Soc. Rev.*, 2015, **44**, 4547–4595.
7 L. Yuan, W. Lin, K. Zheng, L. He and W. Huang, *Chem. Soc. Rev.*, 2013, **42**, 622–661.
8 B. Zhang, C. Ge, J. Yao, Y. Liu, H. Xie and J. Fang, *J. Am. Chem. Soc.*, 2015, **137**, 757–769.
9 J. Wu, I. Hwang, K. S. Kim and J. S. Kim, *Org. Lett.*, 2007, **9**, 907–910.
10 J. B. Birks, *Photophysics of Organic Molecules*, Wiley, New York, 1970.
11 J. R. Lakowicz and B. R. Masters, *J. Biomed. Opt.*, 2008, **13**, 029901.
12 J. Luo, Z. Xie, J. W. Y. Lam, L. Cheng, H. Chen, C. Qiu, H. S. Kwok, X. Zhan, Y. Liu, D. Zhu and B. Z. Tang, *Chem. Commun.*, 2001, 1740–1741.
13 H. Tong, Y. Dong, Y. Hong, M. Häussler, J. W. Y. Lam, N. H. Sung, X. Yu, J. Sun, I. D. Williams, H. S. Kwok and B. Z. Tang, *J. Phys. Chem. C*, 2007, **111**, 2287–2294.
14 G. Sun, Y. Zhao and W. J. Liang, *J. Chem. Theory Comput.*, 2015, **11**, 2257–2267.
15 A. K. Chaudhari, H. J. Kim, I. Han and J. Tan, *Adv. Mater.*, 2017, **29**, 1701463.
16 Y. Cui, Y. Yue, G. Qian and B. Chen, *Chem. Rev.*, 2012, **112**(2), 1126–1162.

17 W. P. Lustig, S. Mukherjee, N. D. Rudd, A. V. Desai, J. Li and S. K. Ghosh, *Chem. Soc. Rev.*, 2017, **46**(11), 3242–3285.
18 A. Fermi, G. Bergamini, M. Roy, M. Gingras and P. Ceroni, *J. Am. Chem. Soc.*, 2014, **136**, 6395–6400.
19 P. Chen, Q. Li, S. Grindy and N. Holten-Andersen, *J. Am. Chem. Soc.*, 2015, **137**, 11590–11593.
20 S. W. Provencher, *J. Chem. Phys.*, 1976, **64**, 2772–2777.
21 X. Zhang, Z. Huo, T. Wang and H. Zeng, *J. Phys. Org. Chem.*, 2012, **25**(9), 754–759.
22 G. GrÖger, W. Meyer-Zaika, C. BÖttcher, F. GrÖhn, C. Ruthard and C. Schmuck, *J. Am. Chem. Soc.*, 2011, **133**, 8961–8971.
23 T. Xie, X. Wu, K. J. Endres, Z. Guo, X. Lu, J. Li, E. Manandhar, M. Ludlow, C. J. Moorefield, M. Saunders, C. Wesdemiotis and G. R. Newkome, *J. Am. Chem. Soc.*, 2017, **139**, 15652–15655.
24 K. Yoshida, N. Oga, T. Koujiri, M. Ishiguro and Y. Kubo, *J. Chem. Soc., Perkin Trans. 1*, 1990, 1891–1895.
25 T. Asano, T. Okada, S. Shinkai, K. Shigematsu, Y. Kusano and O. Manabe, *J. Am. Chem. Soc.*, 1981, **103**, 5161–5165.
26 E. V. Brown and G. R. Granneman, *J. Am. Chem. Soc.*, 1975, **97**, 621–627.
27 T. Asano and T. Okada, *J. Org. Chem.*, 1986, **51**, 4454–4458.
28 K. S. Schanze, T. F. Mattox and D. G. Whitten, *J. Org. Chem.*, 1983, **48**, 2808–2813.
29 J. Henzl, M. Mehlhorn, H. Gawronski, K. Rieder and K. Morgenstern, *Angew. Chem., Int. Ed.*, 2006, **45**, 603–606.
30 A. Cembran, F. Bernardi, M. Garavelli, L. Gagliardi and G. Orlandi, *J. Am. Chem. Soc.*, 2004, **126**, 3234–3243.
31 C. Burger, J. Hao, Q. Ying, H. Isobe, S. Sawamura, E. Nakamura and B. Chu, *J. Colloid Interface Sci.*, 2004, **275**, 632–641.

